ARTICLES

Spectral momentum density of electrons in copper

X. Guo,* Z. Fang, A. S. Kheifets,† S. A. Canney, M. Vos,† and I. E. McCarthy
Electronic Structure of Materials Centre, The Flinders University of South Australia, Adelaide, South Australia 5001, Australia

E. Weigold
Research School of Physical Sciences and Engineering, Institute of Advanced Studies, The Australian National University, Canberra, ACT 0200, Australia

(Received 28 July 1997)

The spectral-momentum density of electrons in a copper thin film has been directly measured using electron momentum spectroscopy. The measured spectral-momentum density shows two distinct features. The first is a free-electron-like parabola with dispersion spanning 10 eV in energy and 0.65 a.u. in momentum. The other is a weak and extended band located in a narrow range of energies from about 2 to 5 eV below the Fermi level. A spherically averaged linear muffin-tin orbital (LMTO) calculation of copper reproduces these features in both the dispersion pattern and the intensity. After taking into account the elastic and inelastic multiple scattering through a Monte Carlo simulation, the agreement between the calculation and the measurement is good. The measurement and the LMTO calculation are also compared with an available linear-augmented-plane-wave calculation for the energy-integrated electron momentum distribution of the valence band and the agreement is also good. [S0163-1829(98)00812-1]

I. INTRODUCTION

The electron spectral-momentum density is the energy-resolved momentum density distribution of electrons in solids, which provides detailed information on the electronic structure of solids. For example, the three-dimensional energy-momentum dispersion pattern of electrons in a solid is obviously contained in the measured spectral momentum density. Over the last ten years electron momentum spectroscopy (EMS) or $(e,2e)$ spectroscopy has developed into a powerful technique to measure directly the electron spectral-momentum density of crystalline solids and, in particular, structurally disordered solids.[1,2]

Electron momentum spectroscopy is based on the $(e,2e)$ reaction.[3] In an $(e,2e)$ experiment all kinematical parameters are accurately measured. These parameters are incident electron kinetic energy E_0 and momentum $\mathbf{p}_0$, scattered electron (*fast* electron) kinetic energy E_f and momentum $\mathbf{p}_f$, and ejected electron (*slow* electron) energy E_s and momentum $\mathbf{p}_s$. At high incoming and outgoing electron energies and large momentum transfer $\mathbf{K}=\mathbf{p}_0-\mathbf{p}_f$, the $(e,2e)$ cross section is dominated by binary collisions of the incident electron and the bound electron in the target. The binding energy ε and momentum $\mathbf{q}$ of the bound electron *before* the collision are then determined via energy and momentum conservation, neglecting the recoil energy of the ion:

$$E_0-\varepsilon=E_f+E_s, \tag{1}$$

and

$$\mathbf{p}_0+\mathbf{q}=\mathbf{p}_f+\mathbf{p}_s, \tag{2}$$

where $\mathbf{q}$ is the *real* momentum of the bound electron.

Within the independent particle approximation the $(e,2e)$ cross section is proportional to the modulus square of the bound electron momentum space wave function $|\phi(\varepsilon,\mathbf{q})|^2$, i.e., the electron spectral momentum density $\rho(\varepsilon,\mathbf{q})$.[4,5] For different kinematic conditions that correspond to different momenta $\mathbf{q}$ and different binding energies ε via Eq. (1) and Eq. (2), the measurement of $(e,2e)$ cross sections is thus a direct measurement of the spectral momentum density $\rho(\varepsilon,\mathbf{q})$ of the bound electrons in the target. Thus the method is commonly referred to as electron momentum spectroscopy. Since the measurement does not rely on the crystal momentum, EMS applies equally to ordered (crystalline) or disordered samples.[5,6]

Conventionally, density of states (DOS) is used to describe the electronic structure of solids. The DOS is proportional to the number of one-electron states (integrated over momentum space) in the energy range from ε to $\varepsilon+d\varepsilon$. Calculated densities are often compared to x-ray photoemission spectroscopy (XPS) spectra. The spectral intensity of a band state as measured by photoemission depends significantly on the dynamics of the process since the cross-section is related to the atomic orbital origins of the band state and the incident energy of the light source.[7] We take the photoemission measurement of CuO as an example.[8] The cross-section ratios, weighted by the number of electrons per atom, are $\sigma(O\ 2p)/\sigma(\mathrm{Cu}\ 3d)\approx 2.16$, 1.05, and 0.03 for He I (21.2 eV), He II (40.8 eV), and XPS (Al$K\alpha$, 1486.6 eV) light sources, respectively. That is, in XPS one has primarily emission of d electrons, whereas in He I and He II spectra one sees more or less equally both d and p electron emissions. Therefore, detailed information on the DOS and on the

electron momentum distribution can not be directly obtained by photoemission measurements. Over the past two decades angle-resolved photoemission spectroscopy (ARPES) has been developed to study the electronic structure of solids, in particular to map the energy, crystal-momentum dispersion relationship. However, ARPES measurements can only be interpreted for crystalline solids, and in any case give no direct information on the momentum density. For structurally disordered solids so far only EMS can provide detailed information on all three aspects, energy, momentum and associated density.

To the best of our knowledge there have been no published experiments on the spectral-momentum density of structurally disordered metals containing *d* electrons in their valence band, although the literature on electronic structure of crystalline forms of these metals is overwhelming.[9] Copper, situated at the end of the first row of transition metals in the periodic table with a filled $3d$ shell and half filled $4s$ shell, is an interesting system to study with EMS. Elemental solids previously studied with EMS all have a valence band consisting of entirely *s* and *p* electrons.[1] The valence band of copper contains *s*, *p*, and *d* electrons. Also, an EMS study of the valence band of copper would build up a basis for EMS studies of transition metals that have partially filled *d* bands. It is known that the properties of the transition metals are to a considerable degree dominated by the behavior of the *d* electrons.

In this paper we report the measurement of the spectral-momentum density of electrons in structurally disordered copper using EMS. These measurements are compared to spherically averaged linear muffin-tin orbital (LMTO) calculation of crystalline copper. The calculation therefore treats the disordered solid as if it were polycrystalline. Although this spherical averaging may not be a perfect way of dealing with the real electronic structure of a disordered target, it provides a very useful starting point to interpret the experimental results and to discuss the roles of the $3d$ electrons in the valence band. To estimate the contributions to the measured result of multiple scattering, stemming from elastic and inelastic collisions, the LMTO calculation is convoluted with these collision processes through a Monte Carlo simulation. The measurement and the LMTO calculation are also compared with a linear-augmented-plane-wave (LAPW) calculation for the energy-integrated electron momentum distribution of the valence band.

II. THEORETICAL MODEL

As in our previous work on disordered materials[10–13] we treat the structurally disordered copper as a spherical average of its crystalline counterpart. We have performed the band structure and momentum density calculations on crystalline copper by employing the linear muffin-tin orbital (LMTO) method in the atomic sphere approximation.[14] We use the local density approximation to the density functional theory with the von Barth and Hedin parametrization for the exchange-correlation potential.[15] Details of the calculated electronic structure of copper are given in Table I. The LMTO method was applied previously to copper by Jepsen *et al.*[16] who calculated the self-consistent potential inside the atomic sphere and used this potential as an input to a more accurate linear-augmented-plane-wave (LAPW) calculation. As can be seen from Table I, our results are in excellent agreement with those of Jepsen *et al.*[16] and are in good agreement with the experimental values collected in a review paper by Courths and Hüfner.[17] A better agreement with a wide range of experimental data obtained by using various sources of low- and high-energy electromagnetic radiation is hardly possible to achieve within an independent particle model. For this purpose a better account for many-electron correlations is required which goes beyond the scope of the present paper.

TABLE I. Band structure parameters of copper.

	Present LMTO	Jepsen *et al.*[a]	Courths and Hüfner[b]
Band energies (eV)			
Γ_1	−9.32	−9.36	−8.60(0.05)
Γ_{12}	−2.30	−2.27	−2.78(0.03)
$\Gamma_{12}-\Gamma_{25}$	0.80	0.75	0.81(0.06)
X_5	−1.53	−1.54	−2.01(0.03)
X_5-X_3	3.03	2.80	2.79(0.06)
X_5-X_1	3.55	3.40	3.17(0.04)
L_3	−1.69	−1.69	−2.25(0.05)
$L_{2'}$	−0.90	−1.10	−0.85(0.10)
L_3-L_3	1.45	1.40	1.37(0.07)
L_3-L_1	3.56	3.29	2.91(0.07)
$L_1-L_{2'}$ (L-gap)	5.98	4.90	4.95(0.10)
Fermi momentum (a.u.)			
k_F (100)	0.78	0.76	0.761
k_F (110)	0.66	0.68	0.683
k_F (L-W) (neck)	0.11	0.15	0.135

[a]Reference 16.
[b]Reference 17.

The momentum density formalism within the LMTO framework was developed by Singh and Jarlborg.[18] In our previous work[19,20] we used essentially the same formalism. However, we neglected a so-called overlap correction arising from the calculation of the Fourier transform by integrating over the Wigner-Seitz sphere rather than the unit cell. This correction is computationally expensive to implement, especially for complex solids with more than one atom per unit cell, but it does not produce a noticeable change to the electron momentum density. However, in the present work on copper, we are able to perform an accurate momentum density calculation which includes the overlap correction.

The results of the energy band and momentum density calculation along several conventional fcc symmetry lines are presented in the top panel of Fig. 1. The valence band of copper is comprised of six individual bands, originating from one *s* and five *d* atomic levels. The orbital character is highlighted in Fig. 1 by the line width with which the bands are drawn. The width is proportional to the modulus squared of the corresponding orbital components in the LMTO eigenvector. The part of the band structure that resembles a free electron parabola has mainly sp character, whereas the bands with only minor dispersion have predominantly *d* character. For convenience we will often use the nomenclature of ''*d* band'' for those bands with mainly *d* character and ''*s*-*p*

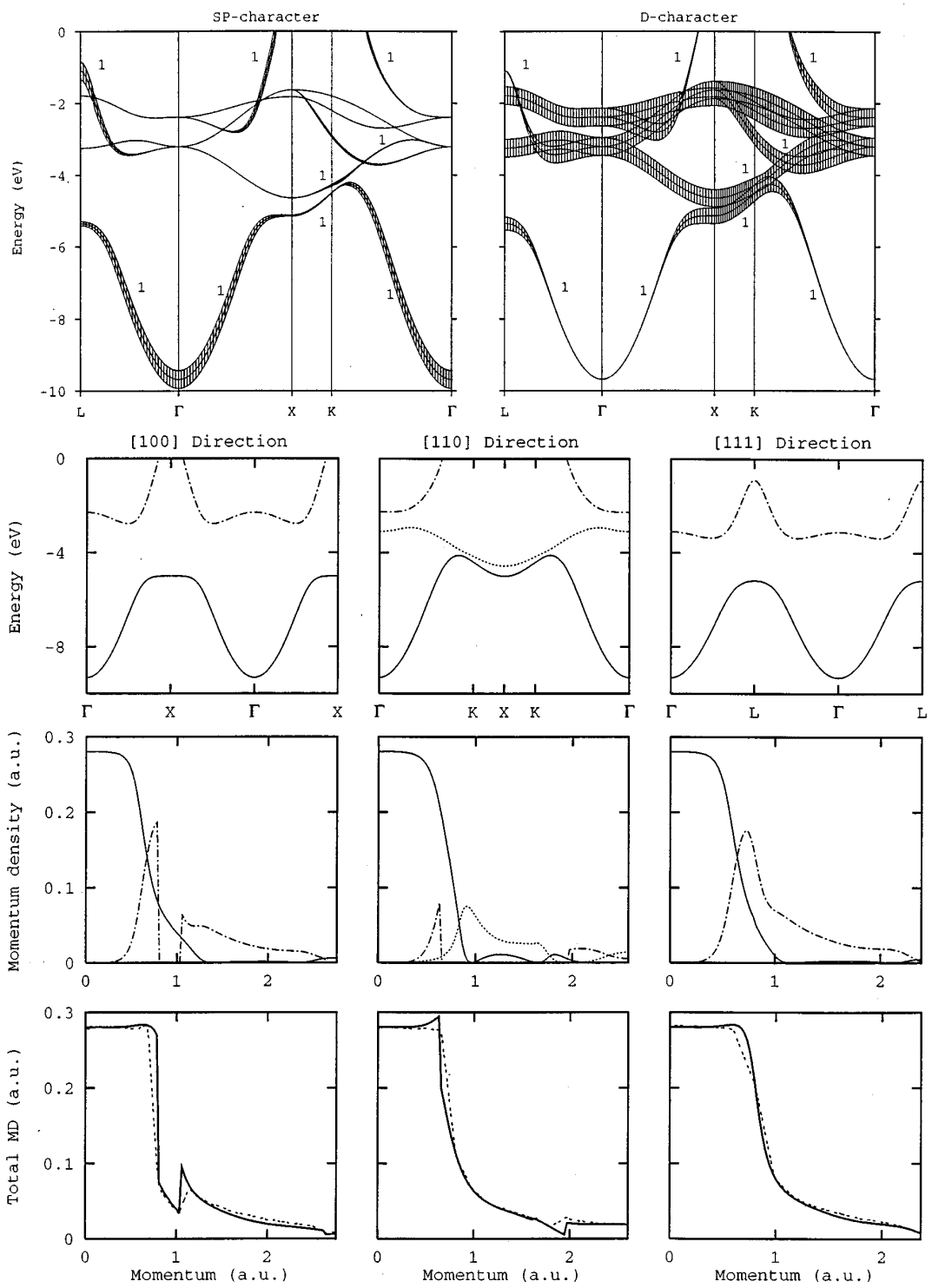

FIG. 1. In the top panel we show the band structure of copper given by the present LMTO calculation. The width of the lines in the left panel is proportional to the *s*-*p* character of the band at the specific momentum, in the right panel it is proportional to the *d* character. The second row shows the band energy along the three main symmetry directions but only for those bands that have nonzero momentum densities along those directions. The third row shows the corresponding band-resolved momentum densities (as indicated by the line styles). The total momentum density summed over the valence band is shown in the bottom panels. The solid line is the present calculation, the dashed line represents the linear-augmented-plane-wave (LAPW) calculation of Papanikolaou (Ref. 22).

band'' for the free-electron-like structure.

For each major crystallographic direction the energy bands are shown in the second panel using the repeated zone scheme. Only bands belonging to the totally symmetric representations, i.e., Γ_1, Δ_1, Σ_1, Λ_1, etc., are plotted. As demonstrated by Harthoorn and Mijnarends[21] only those bands yield a nonzero momentum density along the chosen directions.

The corresponding band-resolved momentum densities are shown in the third panel, using the same line styles as in the second panel. We plot the momentum density versus real momentum **q**. In the first Brillouin zone (first BZ) **q**=**k**,

where **k** is crystal momentum, beyond the first BZ **q**=**k**+**G**, where **G** is a reciprocal lattice vector.

In the three bottom panels of Fig. 1 we compare our calculation for the total, or summed over the all contributing bands, momentum density with the LAPW calculation of Papanikolaou *et al.*[22] Agreement between the two calculations is very good. Any minor deviations could be due to the much coarser momentum grid used as well as an error introduced by digitizing the plot published in Ref. 22.

We should mention another electron momentum density calculation on copper. Mijnarends and Rabou[23] used the Korringa-Kohn-Rostoker (KKR) method. Their results are qualitatively very similar to the present calculation. However, they presented the electron momentum density modulated by the positron wave function and a direct comparison is difficult.

As was mentioned above, to compare our calculation with the experiment we perform a spherical averaging over the irreducible wedge of the BZ. The rigorous averaging technique is described in detail in Ref. 19. Although mathematically correct, this procedure gives little insight into the resulting momentum density which one would expect to be observed in the experiment. For a qualitative analysis it is more transparent to use the plots of Fig. 1 since the irreducible wedge of the fcc BZ is enclosed within the three directions shown in the figure. So the spherically averaged momentum density is expected to be close to an arithmetic average of these three directions.

Near the Γ point the lower band which has predominantly *s* character disperses upwards along a free-electron-like parabola with nearly constant momentum density. This behavior, being fairly isotropic, will survive the spherical averaging and is expected to be seen in the experiment. The uppermost band has almost pure *d* character near the Γ point. It is rather flat and gives very little contribution to the momentum density because of the symmetry of *d* orbitals. However, further away from the Γ point the upper band increases in intensity and disperses upwards before it crosses the Fermi surface in the ΓX and ΓK directions, or turns around in the ΓL direction. This behavior is again quite isotropic and should be visible in the experiment. Combination of the two bands will be seen as a parabola extending from the bottom of the valence band at the Γ point up to the Fermi level which has a gap at a few eV below E_F. This is exactly the picture one would expect from a conventional representation of the band structure of copper as a result of the hybridization of a free-electron-like *s*-*p* band and the atomiclike *d* bands.[24]

At high momenta in the second and third BZ both the lower and upper bands are rather anisotropic and one would expect a fairly broad energy spread of the spherically averaged momentum density. The amplitude of the momentum density is small as compared to the peak intensity observed in the first BZ. This and other predictions of the theory are in fact reproduced very nicely in the experiment which will be discussed in Sec. IV.

III. EXPERIMENTAL DETAILS

The experiment was performed using the EMS spectrometer at The Flinders University of South Australia. A detailed description of the spectrometer is given by Storer *et al.*[25] and Canney *et al.*[26] In brief, the spectrometer is set up in a noncoplanar asymmetric geometry and measurements are made in a transmission mode. A schematic representation of the geometry is shown in Fig. 2. The incident electron energy is 20.8 keV plus the binding energy. The thin film sample is held vertically and positioned at an angle of 30° with respect to the incident beam. The fast and slow electrons have energies of 19.6 keV and 1.2 keV, and are measured in coincidence with two electron analyzers each measuring simultaneously a range of azimuthal angles (out of the plane) and energies at polar angles of 13.6° and 76° respectively. With these kinematics the momentum transfer *K* is about 9.2 a.u. (1 a.u.$=1.89$ Å^{-1}) and the measurement is performed near the Bethe ridge,[27] where the momentum transfer is roughly equal to the square root of the energy transfer and the ionizing process is dominated by the binary collision mechanism. The electron analyzer used for measuring the fast electrons is a hemispherical analyzer with a pass energy of 100 eV; the one for the slow electrons is a toroidal analyzer with a pass energy of 200 eV. By using two-dimensional position sensitive detectors in the analyzers, a range of energies and azimuthal (out of plane) angles of the outgoing electrons, 20 eV and $\pm 18°$ for the hemispherical analyzer, and 36 eV and $\pm 6°$ for the toroidal analyzer, are measured simultaneously. An overall measurable energy range of 56 eV at a given incident energy with a resolution of 0.9 eV and an effective momentum range from -3.0 to 3.0 a.u. with a resolution of better than 0.15 a.u. have been achieved.

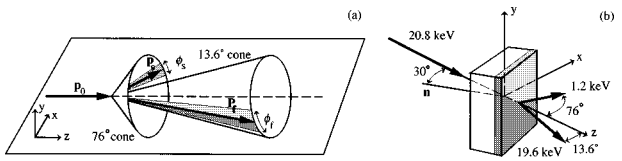

FIG. 2. Schematic representation of the noncoplanar asymmetric geometry used in the EMS measurements. (a) The scattering geometry; (b) the incident and outgoing beams relative to the sample.

The structurally disordered copper sample was prepared in the following way. A dc sputter deposition source (Torus, TRS1CV) was employed to deposit 100 nm of high purity (99.99%) copper onto a NaCl crystal substrate. The 100 nm film was then floated off in distilled water and mounted onto a molybdenum sample holder with 0.7 mm diameter holes. After being dried in air the sample was put into a vacuum chamber. Ion beam thinning was used to thin the film to a thickness that gives a sufficient $(e,2e)$ coincidence count rate. This was done in the ion beam sputtering chamber with a base pressure in the low 10^{-8} Torr range. An rf plasma ion source[28] was used to produce a well focused Ar^+ beam with variable energies from 300 to 1000 eV and a current up to 10 μA. The running pressure was 4×10^{-5} Torr. The Ar^+ beam with an energy of 800 eV was used for initial thinning of the sample. During the thinning process, the change of color of the film was monitored using a telescope to indicate when sufficient thinning had taken place. When the thickness of the sample looked close to that required, the energy of the Ar^+ beam was adjusted to 300 eV to reduce the thinning speed and to prevent the sample from breaking. After thinning the chamber was pumped back down to the base pressure and the sample was transferred under vacuum to a

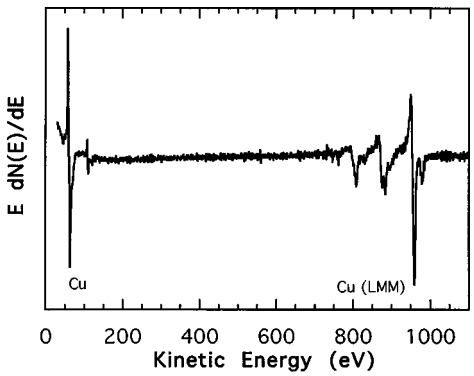

FIG. 3. The Auger electron spectrum for the self-supporting copper sample after ion beam thinning and cleaning showing no signs of contamination.

preparation chamber where an Auger electron spectrum of the sample was taken under ultrahigh vacuum (UHV) conditions to determine the composition of the surface. The sample was then transferred into the main chamber for the EMS measurement. The pressure of the main chamber was maintained at 1.2×10^{-10} Torr during the measurement. An $(e,2e)$ coincidence count rate of 35 counts per minute was achieved. The thickness of this self-supporting sample was estimated to be about 8 nm.

The Auger electron spectrum of the sample measured just before the EMS measurement is shown in Fig. 3. It can be seen that the sample has a clean surface after the Ar^+ beam thinning. Because of the Ar^+ beam bombardment during the thinning process any crystalline structure will be damaged. Therefore, we regard this sample as a polycrystalline copper thin film.

IV. RESULTS AND DISCUSSION

The measured spectral-momentum density of the self-supporting copper thin film and the LMTO calculation on spherically averaged copper are presented in Fig. 4 in the left and middle panels respectively. The LMTO result after the Monte Carlo simulation of the multiple scattering is presented in the right panel in Fig. 4, and will be discussed later. The binding energy shown in this figure is relative to the vacuum level, and the estimated Fermi level position is 4.5 eV below the vacuum level. The highest density in all plots has been normalized to unity. The linear grey scale is shown on the right hand side, the darker the higher density. For easy comparison with the experimental result the LMTO calculation has been convoluted with an energy spread of 1.5 eV and a momentum spread of 0.1 a.u.

In the experiment one can see as a main feature, a free-electron-like parabola intersected a few eV below the Fermi level by a weak, fairly narrow band, spread out in momentum. This weak and extended band shows no obvious dispersion and is considered to be dominated by d electron orbitals. The free-electron parabola, relatively intense near zero momentum seems to disappear in the d band region, but reappears briefly between the top of the d band and the Fermi level, but with reduced intensity. Also the momentum of the free electron feature seems almost independent of energy between the d band region and the Fermi level. All these features are reproduced very well in the LMTO calculation except that the narrow band appears to have slight dispersion.

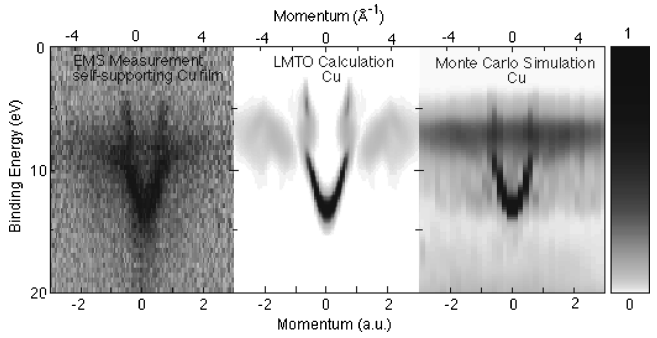

FIG. 4. The spectral momentum density plots as measured with the spectrometer for the self-supporting copper samples compared with a LMTO calculation on a spherically averaged crystalline copper (left and middle panels, respectively). The LMTO result including Monte Carlo simulation of multiple scattering effects is shown in the right panel. The binding energy is relative to the vacuum level. The highest density in each panel has been normalized to unity. The linear grey scale is shown on the right-hand side.

At first appearance at these measured and calculated spectral-momentum density plots, do not seem to match the density of states (DOS) $n(\varepsilon)$ of copper measured by photoemission[29] where the narrow d band dominates the intensity. In an energy band calculation of copper there are six bands that accommodate the eleven electrons $(3d^{10}4s^1)$ in the valence band. Of these six bands five are located in a relatively narrow energy range from 2 to 5 eV below the Fermi level, and a sixth, the s-p band extends from the Fermi level to about 10 eV below the Fermi level (about 14.5 eV below the vacuum level). Therefore the calculation of DOS $n(\varepsilon)$ of copper shows a peak in the narrow d band region superimposed on the weaker intensity in the s-p band region. For an amorphous or a structurally disordered target the density of states $n(\varepsilon)$ and the spectral-momentum density $\rho(\varepsilon,\mathbf{q})$ should be related by

$$n(\varepsilon)=8\pi\int_0^\infty dq q^2\rho(\varepsilon,q). \tag{3}$$

Thus in the DOS the high momentum components of the measured intensity are weighted much more heavily than the measured intensity near zero momentum. Using Eq. (3) one should be able to get $n(\varepsilon)$ from the measured spectral-momentum density $\rho(\varepsilon,q)$ for an amorphous or a structurally disordered target. This works well for elemental solids consisting of s and p electron orbitals such as aluminum[13,30] and germanium,[31] but it does not give a reasonable result for copper and nickel.[32] The reason for this is that both copper and nickel contain d electrons in their valence bands and the d electrons have a large momentum spread that is beyond the limit of the spectrometer (the upper limit of effective measurable momentum is 3 a.u.). So a considerable amount of information required by Eq. (3) is not available. To illustrate this a calculated partial number of electrons with momentum with magnitude between q and $q+\delta q$, where $\delta q=0.2$ a.u. for q varying from 0 to 4 a.u. is shown in Fig. 5. Below 1 a.u. the electrons are mainly from the $4s$ levels. The $3d$ electrons dominate the high momentum region. Even above

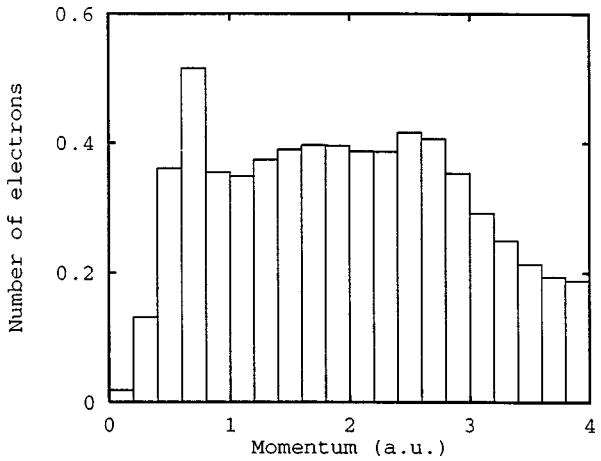

FIG. 5. The calculated partial number of valence electrons in copper in a given momentum range. The total number of electrons from 0 up to 4.0 a.u. is 6.37 as compared with 11 electrons in the full momentum space.

the momentum of 3 a.u. the partial number of electrons is still comparable with that below 1 a.u. on average. As a matter of fact, the integration of the calculated spectral momentum density $\rho(\varepsilon,q)$ using Eq. (3) from 0 to 4 a.u. gives a total number of electrons per atom of $N_e=6.37$ as compared to the 11 electrons actually present. The density of states is heavily weighted by the high momentum components in the spectral-momentum density, as can be seen from the momentum space q^2 weighting in Eq. (3).

For a quantitative comparison between the measurement and the calculation, cuts along the binding energy at intervals of 1 eV are shown in Fig. 6. The data points with error bars are the experimental data. The dashed lines are the results of the LMTO calculation obtained by cutting the calculated spectral momentum density plot in the same way as that for the experimental data.

It is obvious from Fig. 6 that the measured momentum distributions are broader than the calculated ones, even though the major features (peaks) are approximately in accord. This is largely due to elastic scattering in the incoming and outgoing electron channels. In principle there are two ways to compare the measured and calculated electronic structure information in the presence of multiple scattering. One way is to deconvolute the measured data and compare the result to the theory. This approach was followed by Jones and Ritter.[33] The choice of the right response function is complicated by the asymmetric nature of our experiment. The other approach, followed by Vos and Bottema,[34] is to model the multiple scattering using theoretical models and incorporate the result in the theory. Here we use the latter approach. In this approach the assumptions made are more clear, not hidden in the form of the response function used for deconvolution.

We used Monte Carlo simulations of the incoming and outgoing electron trajectories to estimate the probability that one or more of the electrons involved (the incoming, slow and fast outgoing ones) loses energy due to inelastic scattering (mainly plasmon excitations) or experiences a change in momentum (mainly due to scattering from the atom cores). In the simulations the geometry and the kinematics are the same as those shown in Fig. 2 and the thickness of the

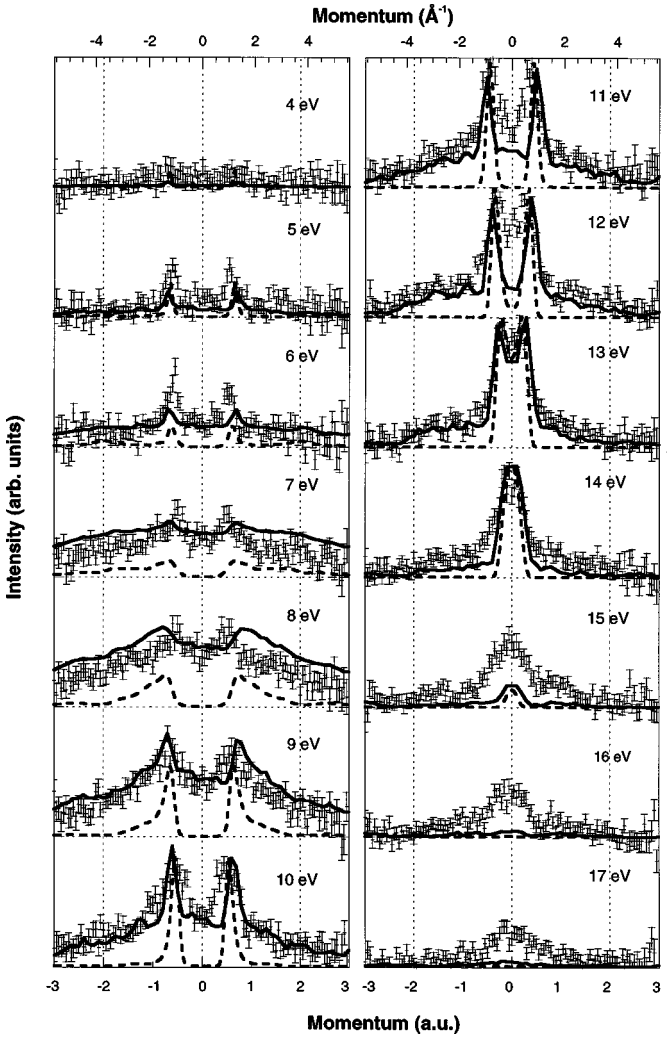

FIG. 6. The momentum distributions at selected binding energies for the valence band of copper. The experimental data are shown as data points with error bars. The dashed curves are results from the LMTO calculation and the solid lines are results of the calculation with Monte Carlo simulation of multiple scattering effects.

sample is assumed to be 8 nm. The depth distribution of the $(e,2e)$ events is chosen homogeneously over the thickness of the film. For each event the path length of the incoming and outgoing electron trajectories is calculated. The energy loss $\Delta\varepsilon$ and momentum transfer $\Delta\mathbf{p}$ are then estimated for each of the trajectories involved using fairly standard procedures in these type of simulations.[35] The elastic differential cross sections were obtained in the Born approximation for electron scattering from copper atoms using Hartree-Fock wave functions and inelastic cross sections were obtained from a model of plasmon excitations in a free electron gas.

Due to the energy loss and momentum transfer these events appear in the measured intensity for ε and $\mathbf{q}$ combinations as inferred from Eqs. (1) and (2) that do not correspond to the ε and $\mathbf{q}$ values of the spectral momentum density properly. Thus, due to inelastic scattering the measured intensity tends to extend to binding energies larger than the maximum binding energies of the valence band and, due to elastic scattering, there is intensity away from the $\mathbf{q}$ values corresponding to the band structure at binding energy ε.

Without multiple scattering we measure electrons with momentum **q** along the y axis of Fig. 2, i.e., the intensity is proportional to $|\phi(\varepsilon,0,q_y,0)|^2$. The Monte Carlo procedure estimates the $\Delta\varepsilon$, $\Delta\mathbf{p}$ combination for each simulated event, and an estimate of the measured intensity is then obtained from $\Sigma|\phi(\varepsilon+\Delta\varepsilon,\Delta p_x,q_y+\Delta p_y,\Delta p_z)|^2$, where the sum extends over a large number of simulated $(e,2e)$ events. The value of $|\phi(\varepsilon+\Delta\varepsilon,\Delta p_x,q_y+\Delta p_y,\Delta p_z)|^2$ was taken from the LMTO calculation.

From this we can see that the result of the simulation is that the ratio of s-p and d related intensity changes. For example, for an $(e,2e)$ event with $\Delta\varepsilon=0$, $\Delta p_x=0$, $\Delta p_y=0$, and $\Delta p_z=2$ a.u. the value of $|\phi(\varepsilon+\Delta\varepsilon,-\Delta p_x,q_y-\Delta p_y,-\Delta p_z)|^2$ is zero for s electrons as these electrons do not extend beyond momentum values of 1 a.u., but $3d$ electrons can still contribute. Thus in the end it *appears* from these simulations that the d intensity has increased relative to the s-p intensity.

The effect of the simulation is a clear improvement of the agreement between the calculation and the experiment as can be seen in Fig. 4 (right panel) and Fig. 6. In Fig. 6 the theory with (solid line) and without (dotted line) multiple scattering was normalized at the bottom of the valence band (14 eV below the vacuum level). The LMTO theory by itself reproduces the peak positions reasonably well, and after incorporation of the multiple scattering effects by the Monte Carlo procedure the shape of the intensity distribution resembles the experimental data quite well. At high binding energy the simulation fails to reproduce the measured intensity. This is not unexpected due to the simple way in which the inelastic energy loss processes are treated and due to expected satellite contributions at these energies due to many-body effects not included in our calculations. The most disturbing discrepancy between experiment and theory, both with and without multiple scattering corrections is the disagreement between measured and calculated position of the momentum peaks near the Fermi level. It seems fairly well established that the s-p band should reach the Fermi level at momentum close to 0.7 a.u. (depending slightly on crystal orientation) and not near 0.6 a.u as in this measurement. The origin of this is not understood.

A comparison between LMTO and LAPW has been made in Sec. II in three high symmetry directions and the agreement is very good. As only the energy-integrated momentum distribution of the valence band is available in the LAPW calculation, we compare the two calculations with our experimental result by integrating the spectral-momentum density of Fig. 4 over energy across the valence band. The resulting energy-integrated density as a function of momentum is plotted in Fig. 7. The LMTO curve and the Monte Carlo simulation result are obtained in the same way. The LAPW curve is an arithmetical average of the momentum densities in three high symmetry directions ΓX, ΓK, and ΓL presented in the bottom panels in Fig. 1. Comparing the curves in Fig. 7, one can see that the LMTO and LAPW agree very well with each other. The difference between the calculations and the measurement is due to multiple scattering effects. Considering the rather crude way in which the multiple scattering effects are taken into account, the agreement between the simulations and experimental data is surprisingly good.

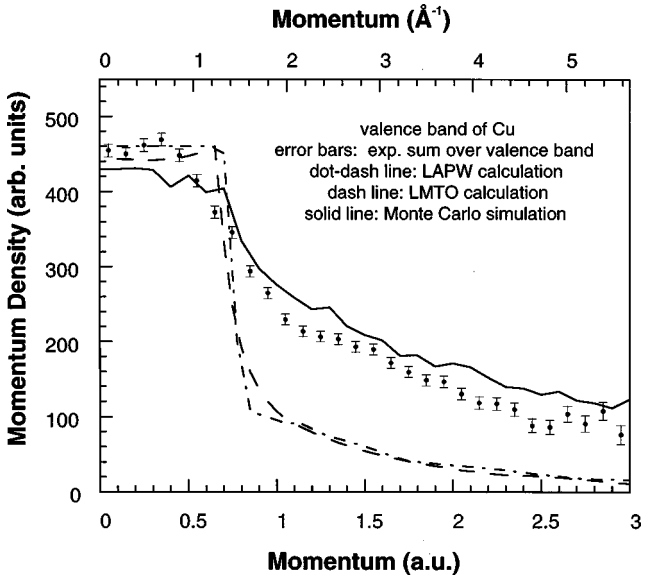

FIG. 7. The momentum density of the valence band in copper. The experimental data (error bars) are obtained by summing over the whole valence band energy range in the spectral momentum density plot; the LMTO calculation without and with Monte Carlo simulation of multiple scattering, shown as the dash line and solid line respectively, are obtained in the same way; the LAPW calculation (dot-dash line) is an arithmetical average of the momentum densities in the three high symmetrical directions ΓX, ΓK, and ΓL presented in the bottom panels of Fig. 1.

It is interesting to notice that, unlike in the spectral momentum density plots of elemental solids C $(2s^2 2p^2, Z=6)$,[36] Al $(3s^2 3p^1, Z=13)$,[13] and Si $(3s^2 3p^2, Z=14)$ (Ref. 37) that show strong intensity at higher binding energies due to plasmon excitation, the spectral momentum density plot of Cu $(3d^{10}4s^1, Z=29)$ [also that of Ni $(3d^8 4s^2, Z=28)$ (Ref. 32)] shows relatively little intensity at higher binding energies. The intensity difference in the higher binding energy region between the two groups of elemental solids can be clearly seen in the momentum-summed (0–2 a.u.) binding spectra shown in Fig. 8. Although exact values are not known, the thickness of these elemental solid samples are all around 8 nm. Why the valence band of Cu and Ni stand out more clearly above the multiple scattering background, compared to the lighter elements is not clear. It could be either related to the higher Z values of Cu and Ni or to the different electronic configuration.

It would be ideal to perform a measurement with a single crystal copper sample so that one can compare directly the calculation and the measurement along chosen symmetry directions. Unfortunately a single crystalline copper sample with a thickness suitable for $(e,2e)$ measurement is not yet available since it requires more sophisticated procedures in the sample preparation.

Finally a remark about the elastic mean free path used in the simulations. In the simulation we performed for copper, the elastic mean free path of the 1.2 keV slow electron, that suffers the most multiple scattering, is only 0.27 nm, comparable to the interatomic distance. In the Monte Carlo simulations we do not take the discrete nature of the lattice into account, and the validity of the procedure followed for cop-

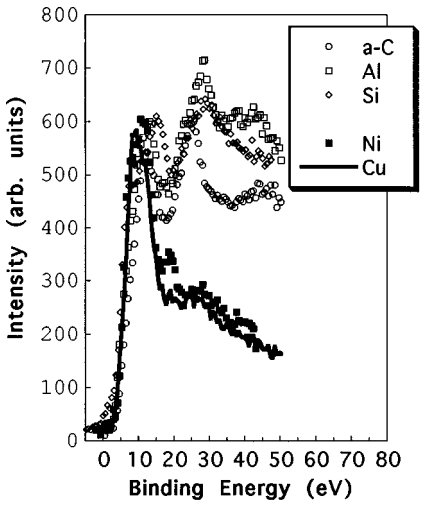

FIG. 8. Comparison of the uncorrected measured binding energy spectra of some elemental solids: amorphous carbon, aluminum, silicon, nickel, and copper. The binding energy spectra are obtained by summing the EMS data over 0–2 a.u. in momentum. The elements can be divided into two groups according to their intensities in the high binding energy region due to inelastic scattering, e.g., plasmon excitation, in the incoming and/or outgoing electrons beams. In the first group (a C, Al, and Si), all elements contain *s* and *p* electron orbitals in their valence band, while the elements in the second group (Cu and Ni) contain *d* electron orbitals as well.

per, and certainly for higher Z materials, is questionable. This problem and all other multiple scattering effects will decrease with increasing energy for the incoming and outgoing electrons. For this purpose a new high-energy spectrometer is under construction.

V. CONCLUSION

The measurement of the spectral-momentum density of electrons in structurally disordered metals containing *d* electrons in their valence bands using EMS has been performed. The metal used in this measurement was structurally disordered copper. The measured result has been compared with an LMTO calculation on spherically averaged crystalline copper. After taking into account elastic and inelastic scattering of the incoming and outgoing electrons by way of Monte Carlo simulation, the calculation reproduces quite well the measurement in both the dispersion pattern and the intensity. However, several differences between theory and the experiment still exist. The *s*-*p* band, which is approximately parabolic in shape, is narrower in momentum space than that indicated by theory. The intensity distribution within the band is quite well described by theory. The measured *d* band structure does not appear to disperse in energy as much as that predicted by the calculation, but the dispersion may be washed out due to the large multiple scattering contribution in this region.

ACKNOWLEDGMENTS

The authors want to thank the technical staff in the Electronic Structure of Materials Centre for their skillful technical support throughout the experiment. Thanks also go to Dr. Q. Qian for assistance in assembling the sputtering chamber for preparing the copper samples during his visit to the Electronic Structure of Materials Centre. The helpfulness of Mr. N. Clisby in running the Monte Carlo simulation program is also acknowledged. This work was supported by a grant from the Australian Research Council.

*Present address: Department of Physics, California State University, Fullerton, CA 92834-9480.

†Present address: Atomic and Molecular Physics Laboratories, Research School of Physical Sciences and Engineering, IAS, The Australian National University, Canberra, ACT 0200, Australia.

[1] E. Weigold, Y. Q. Cai, S. A. Canney, A. S. Kheifets, I. E. McCarthy, P. Storer, and M. Vos, Aust. J. Phys. **49**, 543 (1996).

[2] J. R. Dennison and A. L. Ritter, J. Electron Spectrosc. Relat. Phenom. **77**, 99 (1996).

[3] E. Weigold and I. E. McCarthy, Adv. At. Mol. Phys. **14**, 127 (1978).

[4] I. E. McCarthy and E. Weigold, Rep. Prog. Phys. **54**, 789 (1991).

[5] L. J. Allen, I. E. McCarthy, V. W. Maslen, and C. J. Rossouw, Aust. J. Phys. **43**, 453 (1990).

[6] M. Vos, Z. Fang, S. Canney, A. S. Kheifets, I. E. McCarthy, and E. Weigold, Phys. Rev. B **56**, 963 (1997).

[7] P. M. Williams, *Photoemission Studies of Materials with Layered Structures*, edited by P. A. Lee (Reidel, Dordrecht, Holland, 1976), p. 273.

[8] H. Eskes, L. H. Tjeng, and G. A. Sawatzky, Phys. Rev. B **41**, 288 (1990).

[9] R. Courths and S. Hüfner, Phys. Rep. **112**, 53 (1984).

[10] X. Guo, S. Canney, A. S. Kheifets, M. Vos, Z. Fang, S. Utteridge, I. E. McCarthy, and E. Weigold, Phys. Rev. B **54**, 17943 (1996).

[11] P. Storer, Y. Q. Cai, S. A. Canney, S. A. C. Clark, A. S. Kheifets, I. E. McCarthy, S. Utteridge, M. Vos, and E. Weigold, J. Phys. D **28**, 2390 (1996).

[12] Y. Q. Cai, P. Storer, A. S. Kheifets, I. E. McCarthy, and E. Weigold, Surf. Sci. **358**, 427 (1996).

[13] S. A. Canney, M. Vos, A. S. Kheifets, N. Clisby, I. E. McCarthy, and E. Weigold, J. Phys.: Condens. Matter **9**, 1931 (1997).

[14] H. L. Skriver, *The LMTO Method* (Springer-Verlag, Berlin, 1984).

[15] U. von Barth and L. Hedin, J. Phys. C **5**, 1629 (1972).

[16] O. Jepsen, D. Glötzel, and A. R. Mackintosh, Phys. Rev. B **23**, 2684 (1981).

[17] R. Courths and S. Hüfner, Phys. Rep. **112**, 53 (1984).

[18] A. K. Singh and T. Jarlborg, J. Phys. F **15**, 727 (1978).

[19] A. S. Kheifets and Y. Q. Cai, J. Phys. C **7**, 1821 (1995).

[20] A. S. Kheifets and M. Vos, J. Phys. C **7**, 3895 (1995).

[21] R. Harthoorn and P. E. Mijnarends, J. Phys. F **8**, 1147 (1978).

[22] N. I. Papanikolaou, N. C. Bacalis, and D. A. Papaconstantopoulos, *Handbook of Calculated Electron Momentum Distributions, Compton Profiles, and X-ray Form Factors of Elemental Solids* (CRC, Boca Raton, FL, 1991).

[23] P. E. Mijnarends and L. P. L. M. Rabou, J. Phys. F **16**, 483 (1986).

[24] N. W. Ashcroft and N. D. Mermin, *Solid State Physics* (Holt, Rinehart and Winston, New York, 1976), Chap. 15.

[25] P. Storer, R. S. Caprari, S. A. C. Clark, M. Vos, and E. Weigold, Rev. Sci. Instrum. **65**, 2214 (1994).

[26] S. A. Canney, M. J. Brunger, I. E. McCarthy, P. J. Storer, S. Utteridge, M. Vos, and E. Weigold, J. Electron Spectrosc. Relat. Phenom. **83**, 65 (1997).

[27] M. Inokuti, Rev. Mod. Phys. **43**, 297 (1971).
[28] Z. Fang, X. Guo, S. Utteridge, S. Canney, M. Vos, I. E. McCarthy, and E. Weigold, Rev. Sci. Instrum. **68**, 4396 (1997).
[29] S. Hüfner and G. K. Wertheim, Phys. Lett. **47A**, 349 (1974).
[30] A. S. Kheifets (private communication).
[31] Y. Q. Cai, P. Storer, A. S. Kheifets, I. E. McCarthy, and E. Weigold, Surf. Sci. **334**, 276 (1995).
[32] Q. Qian *et al.* (unpublished).
[33] R. Jones and A. L. Ritter, J. Electron Spectrosc. Relat. Phenom. **40**, 285 (1986).
[34] M. Vos and M. Bottema, Phys. Rev. B **54**, 5946 (1996).
[35] R. Shimizu and Z-J Ding, Rep. Prog. Phys. **55**, 487 (1992).
[36] M. Vos, P. Storer, Y. Q. Cai, I. E. McCarthy, and E. Weigold, Phys. Rev. B **51**, 1866 (1995).
[37] M. Vos, P. Storer, Y. Q. Cai, A. S. Kheifets, I. E. McCarthy, and E. Weigold, J. Phys.: Condens. Matter **7**, 279 (1995).